MICRO- AND MACRO-SCOPIC STUDY OF TWO-PHASE FLOW ON A STEPPED CHUTE

Youichi YASUDA
Dept of Civil Eng., College of Science and Technology, Nihon University, Tokyo 101-8303, Japan - Fax: (81 3) 3259 0409 - Email: yokyas@civil.cst.nihon-u.ac.jp
and Hubert CHANSON
Dept of Civil Engineering, The University of Queensland, Brisbane QLD 4072, Australia
Fax: (61 7) 33 65 45 99 - E-mail: h.chanson@mailbox.uq.edu.au

Abstract : Stepped chute flows are characterised by intense turbulence and strong flow aeration (Fig. 1), but most studies did not investigate the turbulence characteristics. Detailed air-water flow properties were measured in skimming flow on a stepped chute ($\theta = 16^o$, h = 0.05 m). Longitudinal oscillations of depth-averaged flow properties were observed with a wave length of about two step cavity lengths. High turbulence levels were recorded downstream of inception, and the data were correlated to the air-water interface area. In the bubbly flow region ($C < 0.3$), bubble size distributions demonstrated a broad range of entrained bubbles, with a fair proportion associated with a bubble cluster structure. Overall the results emphasise the complexity of air-water skimming flows down stepped chutes.
Keywords : air-water flow, intrusive measurements, velocity distribution, turbulence, bubble sizes, cluster structure

INTRODUCTION

During the last two decades, research onto the hydraulics of stepped chutes was driven by needs for better design guidelines (OHTSU and YASUDA 1998, MINOR and HAGER 2000, CHANSON 2001). Although stepped chute flows are characterised by intense turbulence and strong flow aeration (Fig. 1), most studies did not investigate the turbulence characteristics, at the exception possibly of the works of OHTSU and YASUDA (1997) and CHANSON and TOOMBES (2002). In this study, detailed air-water flow measurements were conducted at the sub-millimetric scale. The data were processed using a state-of-the-art analysis to provide new insights into the bubbly flow structure and turbulence field. The results yield an improved understanding of basic flow structures and macroscopic flow characteristics, associated with a comprehensive measurement methodology.

EXPERIMENTAL FACILITY

Experiments were conducted at the University of Queensland in a 4-m long, 1-m wide, 15.9º slope chute (Fig. 1). Waters were supplied from a large feeding basin (1.5-m deep, surface area 6.8 m × 4.8 m) leading to a sidewall convergent with a 4.8:1 contraction ratio. The test section consisted of a broad-crested weir (1-m wide, 0.88-m long, with upstream rounded corner (0.057-m radius)) followed by eighteen identical steps (h = 0.05 m, l = 0.175 m) made of marine ply. The flow rate was delivered by a pump controlled with an adjustable frequency AC motor drive, enabling an accurate discharge adjustment in a closed-circuit system. The discharge was measured from the upstream head above crest with an accuracy of about 2%. Clear-water flow depths were measured with a point gauge.

Air-water flow properties were measured using a dual-tip conductivity probe developed at the University of Queensland ($\varnothing$ = 0.025 mm, tip separation: 7.8 mm). The probe sensors were aligned in the flow direction and excited by an air bubble detector (AS25240). The velocity

measurements were the longitudinal component of air-water interfacial velocity. The probe signal was scanned at 20 kHz for 20 s at each point. The translation of the probe in the direction normal to the channel invert was controlled by a fine adjustment travelling mechanism connected to a Mitutoyo™ digimatic scale unit (Ref. No. 572-503). The error on the vertical position of the probe was less than 0.025 mm. The accuracy on the longitudinal position of the probe was estimated as $\Delta x < +/- 0.5$ cm. The accuracy on the transverse position of the probe was less than 1 mm.

Table 1 - Summary of experimental results (measurements at step edges)

Step No.	s/d_c	Y_{90}/d_c	C_{mean} $(0\text{-}Y_{90})$	V_{90}/V_c	$\frac{F_{max}*d_c}{V_c}$	$a_{mean}*d_c$ $(0\text{-}Y_{90})$	Remarks
6-7	11.8	--	0.00	--	--	--	Inception point.
7	12.8	0.445	0.24	2.72	6.69	9.55	
9	17.1	0.432	0.30	2.85	10.66	14.47	
10	19.3	0.509	0.26	2.88	13.87	19.47	
11	21.4	0.603	0.35	2.80	14.61	20.86	
12	23.6	0.540	0.28	2.95	18.64	26.62	
13	25.7	0.617	0.39	2.87	17.81	25.42	
14	27.8	0.486	0.23	3.21	19.46	27.78	
15	30.0	0.643	0.37	2.95	17.94	25.08	
16	32.1	0.553	0.28	3.01	21.13	29.67	
17	34.3	0.597	0.37	2.95	19.73	27.71	

Notes : a_{mean} : depth-averaged air-water specific interface area; F_{max} : maximum bubble count rate; s : streamwise distance measured from first step edge.

Fig. 1 - Photograph of the experimental facility ($d_c/h = 1.7$, $h = 0.05$ m, $\theta = 15.9°$)

Data processing

The basic probe outputs are the air concentration, or void fraction C, that is the proportion of time that the probe tip is in the air, and the bubble count rate F that is the number of bubbles impacting the probe tip per second. The velocity measurement V is based upon the successive detection of air-water interfaces by two tips using a cross-correlation technique (e.g. CROWE et al. 1998, CHANSON 2002) (Fig. 2). The shape of the cross-correlation function provides

further information on the velocity fluctuations : i.e., the turbulent intensity Tu derives from the broadening of the cross-correlation function compared to the auto-correlation function (CHANSON and TOOMBES 2002). The probe signals provide further bubble and droplet chord size distributions. The measurement of air-water interface area may be derived from the chord size distributions and by continuity for the air phase (a = 4*F/V).

Flow conditions

Experimental observations were conducted for one flow rate (0.0776 m^3/s) corresponding to a skimming flow regime. The inception point of air entrainment was observed between the 6th and 7th step edges. Detailed air-water flow properties were recorded at each step edge downstream (Table 1). The flow was rapidly varied for $s/d_c < 24$, and quasi-uniform flow conditions were observed for $s/d_c \geq 24$. However true uniform equilibrium flow conditions were not achieved (see Discussion).

Fig. 2 - Dimensionless air-water flow velocity distributions - Comparison with 1/9th power law and clear-water flow turbulence data (u'/V, v'/V) by OHTSU and YASUDA (1997)
Black symbols : velocity in rapidly varied flow - White symbols : velocity in quasi-uniform flow - Grey symbols: Tu in rapidly varied flow- Cross symbols : Tu in quasi-uniform flow

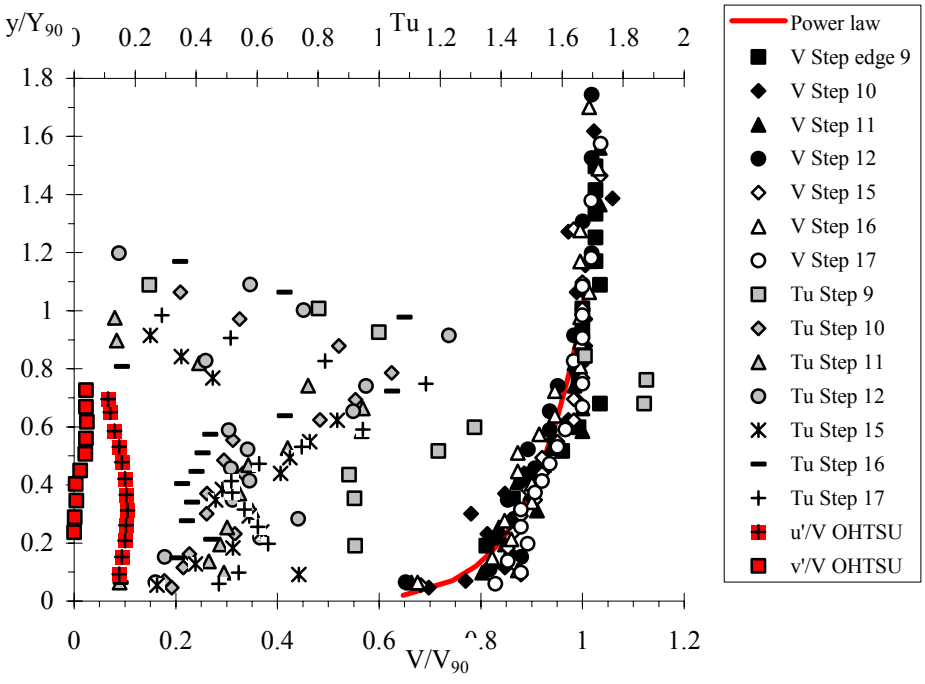

AIR-WATER FLOW PROPERTIES

Air-water velocity measurements at step edges may be re-arranged according to the dimensionless relationship:

$$V/V_{90} = f(y/Y_{90}, h/d_c, h/l, s/d_c) \quad (1)$$

where V_{90} is the characteristic velocity for $y = Y_{90}$, Y_{90} the distance perpendicular to the pseud-bottom formed by the step edges where the void fraction C equals 0.90, d_c the critical depth, h the step height and l the step length. Self-similar velocity distributions were observed (Fig. 2). For $0.05 \leq y/Y_{90} \leq 1$, the distribution was approximated as the 1/9th power law (solid line, Fig. 2). For $1 \leq y/Y_{90} \leq 1.9$ (i.e. $0.9 \leq C \leq 0.995$), the time-averaged velocity increased slightly with increasing distance y/Y90. In that range, a lot of splashing and water

droplets were carried downstream, although the resistance between the spray and the air-water mainstream might be small. Note that a smooth velocity profile was not obtained at each section (Fig. 2). It is believed that three-dimensional turbulent structures and vortex shedding might affect the mean velocity profile in the aerated flow region.

The distributions of turbulence intensity Tu exhibited high turbulence levels across the entire air-water flow mixture (i.e. $0 \leq y \leq Y_{90}$) (Fig. 2). The trend differed significantly from turbulent intensity profiles in boundary layers, but it was consistent with clear-water flow LDV measurements by OHTSU and YASUDA (1997) on a 19º stepped chute (h = 0.05 m), immediately upstream of air entrainment inception. Deviations were maximum for C = 0.4 to 0.6 for all sections. Note high turbulence levels immediately downstream of inception point caused by the formation of strong turbulent structures (Fig. 2).

Fig. 3 - Dimensionless air concentration and bubble count rate distributions - Comparison with Equation (2)
Black symbols : void fraction in rapidly varied flow - White symbols : void fraction in quasi-uniform flow - Grey symbols: bubble count rate in rapidly varied flow- Cross symbols : bubble count rate in quasi-uniform flow

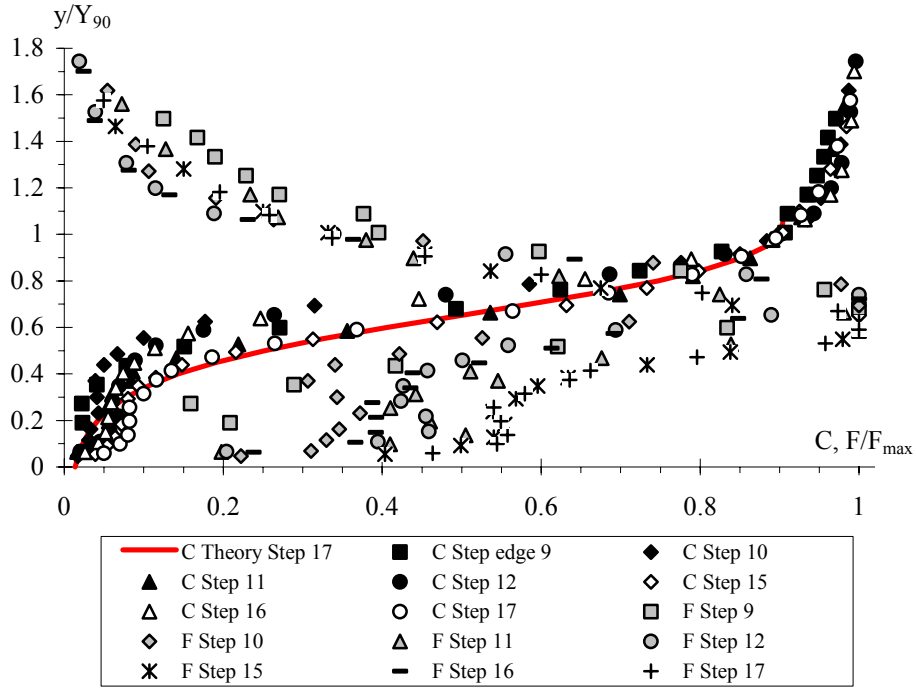

Dimensionless distribution of air concentration C and bubble count rates F/F_{max} are presented in Figure 3. Near the downstream end (i.e. quasi-uniform flow region, $s/d_c \geq 24$), the profiles were basically self-similar and followed closely an analytical solution of the air bubble diffusion equation :

$$C = 1 - \tanh^2\left(K'' - \frac{\frac{y}{Y_{90}}}{2 * D_o} + \frac{\left(\frac{y}{Y_{90}} - \frac{1}{3}\right)^3}{3 * D_o}\right) \qquad (2)$$

where K' and D_o are functions of C_{mean} only (CHANSON and TOOMBES 2002). Equation (2) is compared with the data at the last step edge (Fig. 3). In the quasi-uniform flow region ($s/d_c \geq 24$), the bubble count rate F distributions exhibited a maximum for y/Y_{90} = 0.6 to 0.7 (Fig. 3). For $s/d_c < 24$ (i.e. non-uniform flow region), smaller count rates and a different

distribution pattern were observed at each cross-section, while the location where the bubble count rate was higher than that in the quasi-uniform flow region.

Discussion

It is believed that high turbulence levels were directly caused by air bubble entrainment. Figure 4 presents the dimensionless relationship between specific interface area a and turbulence intensity Tu. At each cross-section, the data showed a monotonic increase in turbulence intensity with increasing interfacial area which may be correlated by :

$$Tu - 0.25 \propto (a * d_c)^n \quad (3)$$

where n is about 1.5 to 3 for the data. Equation (3) is shown in Figure 4 for two cross-sections. For low interface areas (i.e. $a*d_c < 5$), Equation (3) tends to $Tu \approx 0.25$ that is close to OHTSU and YASUDA's (1997) data in clear water stepped chute flow (Fig. 2).

Fig. 4 - Relationship between turbulence intensity and specific interface area - Comparison with Eq. (3) - Black symbols : void fraction in rapidly varied flow - White symbols : void fraction in quasi-uniform flow

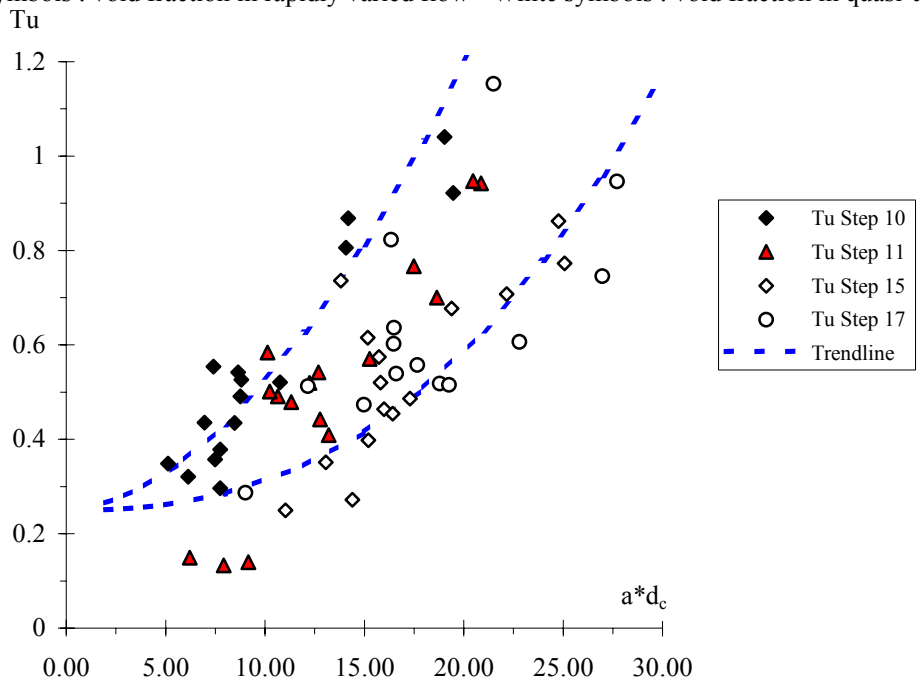

BUBBLE CHORD LENGTH DISTRIBUTIONS AND CLUSTERING EFFECT

Air and water chord lengths were measured in the streamwise direction. Figure 5 presents normalised probability distribution functions of bubble chord sizes at three step edges for an almost identical void fraction. Each data point represents the probability of bubble chord length in 0.5 mm intervals. The probability of chord lengths larger than 15 mm is not shown. The results (Fig. 5) highlight a wide range of bubble chord sizes. The chord length distributions were skewed with a preponderance of small chord sizes relative to the mean. The probability of air bubble chord lengths was the largest for bubble sizes between 0 and 2.5 mm in the bubbly flow region ($C < 0.3$, Fig. 5). It is worth noting some difference in shape and median values between data in non-uniform flow region (Steps 10 & 13) and in quasi-uniform flow region (Step 17). In the spray region ($C > 0.7$), water droplet chord distributions presented flatter distributions than bubble chord distributions in the bubbly flow region ($C < 0.3$). The broad range of bubble and droplet sizes was associated with measured specific

interface areas ranging from 60 to 350 m^{-1} with depth-average specific interface area up to 220 m^{-1} (Table 1).

In the bubbly flow region (C < 0.3), water chord length data provided further information on the streamwise distribution of bubbles and the existence of particle cluster. In a cluster, the bubbles are close together and the packet is surrounded by a sizeable volume of water. For C < 0.3, the analysis of water chord size distributions demonstrated water chord PdF skewed with a preponderance of small water chords compared to the mean. The significant proportion of small water chord sizes corresponded to a number of bubble cluster structures. Two successive bubbles were defined as a cluster when the trailing bubble was separated from the lead particle by a water chord length smaller than one leading bubble diameter. That is, the trailing particle was in the near-wake of the lead bubble. Results are summarised in Table 2. They demonstrated a large proportion (i.e. about 35%) of bubbles travelling as part of a cluster structure. About 70% of clusters consisted of 2 particles only (Table 2). The results suggested a greater number of clusters with numerous bubbles in the quasi-uniform flow region (Table 2, last row). The existence of bubble clusters may be related to breakup, coalescence, bubble wake interference and to other processes. As the bubble response time is significantly smaller than the characteristic time of the flow, it is believed that bubble trapping in large-scale turbulent structures may be another clustering mechanism in bubbly flows. It must be noted that this analysis was conducted along a streamline. It did not consider bubbles travelling side by side as being a cluster.

Fig. 5 - Probability distribution functions of bubble chord sizes in bubbly flow (C < 0.3)

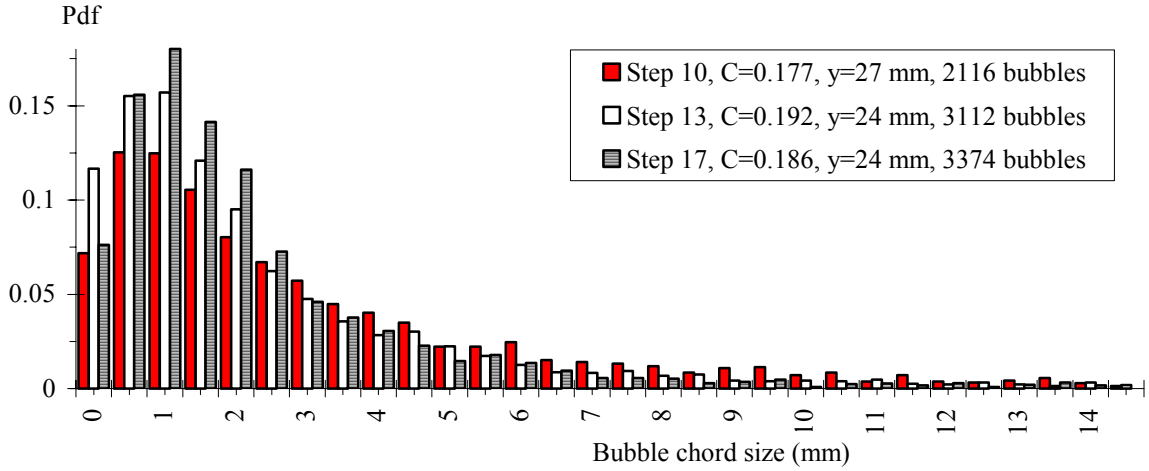

Table 2 - Cluster analysis results in bubbly flow region (C < 0.3)

	Step 10	Step 13	Step 15	Step 17
Total Nb of bubbles	12,591	22,753	22,747	25,955
Total Nb of clusters	1503	3422	3090	3873
% cluster with 2 bubbles	0.780	0.728	0.743	0.706
% cluster with 3 bubbles	0.148	0.185	0.178	0.194
% cluster with 4 bubbles	0.046	0.057	0.054	0.058
% cluster with 5 bubbles	0.012	0.019	0.016	0.025
% cluster with more than 5 bubbles	0.0044	0.0103	0.0087	0.0161

Fig. 6 - Longitudinal dimensionless distributions of mean air content, maximum count rates, characteristic air-water depth Y_{90} and velocity V_{90} - Measurements conducted at step edges

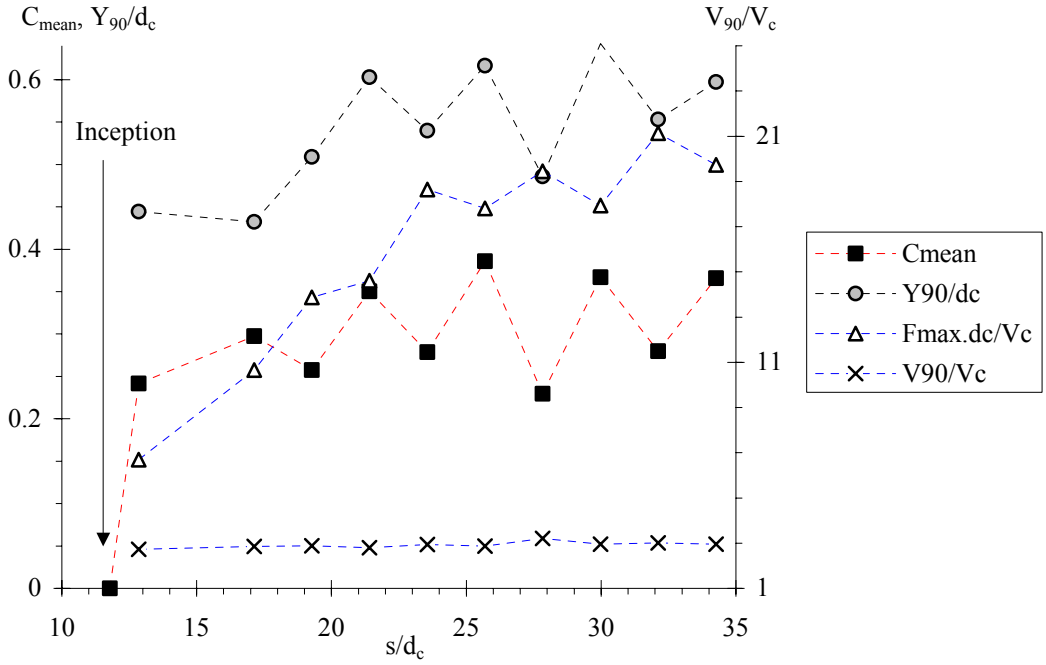

DISCUSSION

Experimental results showed consistently longitudinal fluctuations (oscillations) of flow properties from one step edge to the next one (Table 1, Fig. 6). Similar observations were noted for θ = 53°, 22° and 16° by MATOS (2000), CHANSON and TOOMBES (2002) and GONZALEZ (2003) respectively. Figure 6 presents longitudinal distributions of mean air content C_{mean}, dimensionless air-water depth Y_{90}/d_c, air-water velocity V_{90}/V_c and maximum bubble count rate $F_{max}*d_c/V_c$, where d_c and V_c are the critical depth and velocity respectively, and F_{max} is the maximum bubble count. Although the mean velocity and characteristic velocity V_{90} seem to achieve some equilibrium value, the results exhibit a distinct seesaw pattern with wave length of about two step cavities (Fig. 6). It is believed that these oscillations result from strong interference between vortex shedding in the shear layers behind each step edge and the free-surface (Fig. 7). Flow resistance estimate, calculated between two adjacent step edges, may mis-represent grossly the friction slope. In Figure 6, the calculated friction slope would range between 0.1 to 0.4 for an average value S_f = 0.20. CHANSON et al. (2002) discussed specifically flow resistance data scatter while they proposed an analytical expression of form drag generated by step cavity flows.

Figure 7

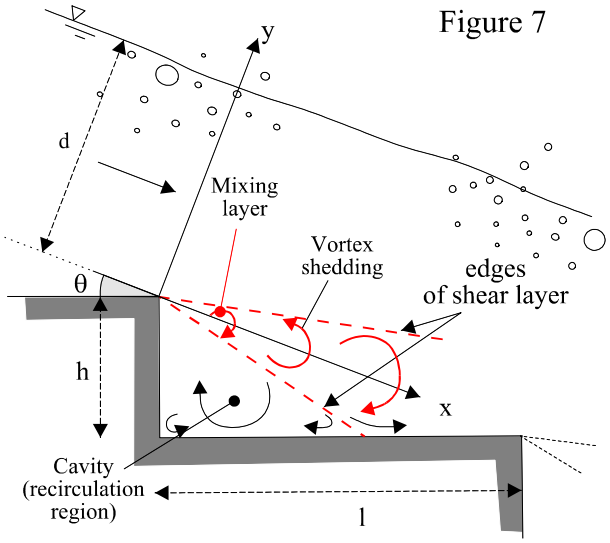

In the non-uniform flow region ($s/d_c < 24$), the dimensionless maximum bubble count rate increased sharply with longitudinal distance s/d_c (Fig. 6). For $s/d_c \geq 24$, there was a marked change in trend, although F_{max} continued to increase gradually with

increasing distance.

SUMMARY AND CONCLUSION

Detailed air-water flow properties, including turbulence and bubble sizes, were measured in skimming flow down a stepped chute (θ = 16º, h =0.05 m). Immediately downstream of the inception point of air entrainment, the flow is rapidly varied ($s/d_c < 24$). Further downstream, although the data showed smooth distributions of void fractions and velocities, longitudinal oscillations of depth-averaged flow properties were observed with a wave length of about two step cavity lengths, while interfacial properties exhibited a gradual, gentle increase with downstream distance. High turbulence levels were recorded downstream of inception. The distributions of turbulence intensity had a similar shape as clear-water flow data of OHTSU and YASUDA down a stepped chute. A strong correlation between turbulence levels and air-water interface area was observed (Eq. (3), Fig. 4).

In the bubbly flow region ($C < 0.3$), bubble size distributions demonstrated a broad range of entrained bubbles and the probability of bubble chord sizes was the largest for chords between 0 and 2.5 mm. A fair proportion (1/3rd) of bubbles were associated with a cluster structure. Most clusters (2/3rd) consisted of two bubbles only. Overall the results emphasise the complexity of air-water skimming flows down stepped chutes. Although the study was limited to one slope, the findings were consistent with previous studies conducted slopes ranging from 16º to 55º. Overall the study proposes a comprehensive methodology for detailed air-water flow measurements which should become the standard for future investigations.

ACKNOWLEDGMENTS

The writers thank Mr C. GONZALEZ (UQ) and Professor Iwao OHTSU (NH) for their help. They acknowledge the assistance of Dr L. TOOMBES (UQ).

REFERENCES

CHANSON, H. (2001). "The Hydraulics of Stepped Chutes and Spillways." *Balkema*, Lisse, The Netherlands, 418 pages.

CHANSON, H. (2002). "Air-Water Flow Measurements with Intrusive Phase-Detection Probes. Can we Improve their Interpretation ?." *Jl of Hyd. Engrg.*, ASCE, Vol. 128, No. 3, pp. 252-255.

CHANSON, H., and TOOMBES, L. (2002). "Air-Water Flows down Stepped chutes : Turbulence and Flow Structure Observations." *Intl Jl of Multiphase Flow*, Vol. 27, No. 11, pp. 1737-1761.

CHANSON, H., YASUDA, Y., and OHTSU, I. (2002). "Flow Resistance in Skimming Flows and its Modelling." *Can Jl of Civ. Eng.*, Vol. 29, No. 6, pp. 809-819.

CROWE, C., SOMMERFIELD, M., and TSUJI, Y. (1998). "Multiphase Flows with Droplets and Particles." *CRC Press*, Boca Raton, USA, 471 pages.

GONZALEZ, C.A. (2003). "Experimental Study of Free-Surface Aeration and Turbulent Processes occurring down an Embankment Dam Stepped Spillway." *Proc. 30th IAHR Biennial Congress*, Student Paper, Thessaloniki, Greece, 8 pages.

MATOS, J. (2000). "Hydraulic Design of Stepped Spillways over RCC Dams." *Proc. Intl Workshop on Hydraulics of Stepped Spillways*, Zürich, Switzerland, Balkema Publ., pp. 187-194.

MINOR, H.E., and HAGER, W.H. (2000). "Hydraulics of stepped spillways." *Proc. Intl Workshop on Hydraulics of Stepped Spillways*, Balkema, The Netherlands.

OHTSU, I., and YASUDA, Y. (1997). "Characteristics of Flow Conditions on Stepped Channels." *Proc. 27th IAHR Biennal Congress*, San Francisco, USA, Theme D, pp. 583-588.

OHTSU, I., and YASUDA, Y. (1998). "Hydraulic Characteristics of Stepped Channel Flows." *Workshop on Flow Characteristics around Hydraulic Structures and River Environment*,

University Research Center, Nihon University, Tokyo, Japan, November, 55 pages.